Journal of Power Sources 268 (2014) 459–468

Contents lists available at ScienceDirect

Journal of Power Sources

journal homepage: www.elsevier.com/locate/jpowsour

Model based condition monitoring in lithium-ion batteries

Amardeep Singh, Afshin Izadian, Sohel Anwar*

Purdue School of Engineering and Technology, IUPUI, Indianapolis, USA

HIGHLIGHTS

- Robust condition monitoring of Li-Ion cell using multiple model adaptive estimation.
- Equivalent circuit based model was updated with a nonlinear OCV–SOC relationship.
- The OCV–SOC equation was obtained via curve fitting of the experimental data.
- The model bank includes a normal cell and two distinctively over-discharged cells.
- RLS method was used to identify the model parameters from measured data.

ARTICLE INFO

Article history:
Received 14 January 2014
Received in revised form
5 May 2014
Accepted 9 June 2014
Available online 17 June 2014

Keywords:
Lithium ion
Analytical redundancy
Extended Kalman filter
Multiple model adaptive estimation (MMAE)
System identification

ABSTRACT

In this paper, a model based condition monitoring technique is developed for lithium-ion battery condition monitoring. Here a number of lithium-ion batteries are cycled using two separate over discharge test regimes and the resulting shift in battery parameters is recorded. The battery models are constructed using the equivalent circuit methodology. The condition monitoring setup consists of a model bank representing the different degree of parameter shift due to overdischarge in the lithium ion battery. Extended Kalman filters (EKF) are used to maintain increased robustness of the condition monitoring setup while estimating the terminal voltage of the battery cell. The information carrying residuals are generated and evaluation process is carried out in real-time using multiple model adaptive estimation (MMAE) methodology. The condition evaluation function is used to generate probabilities that indicate the presence of a particular operational condition. Using the test data, it is shown that the performance shift in lithium ion batteries due to over discharge can be accurately detected.

1. Introduction

Lithium ion (li-ion) batteries are the electrochemical energy source of choice today. A typical li-ion rechargeable cell with lithium metal oxide based positive electrode, graphitic carbon negative electrode, and lithium conducting organic electrolyte, offers great advantages over other battery chemistries [1,2]. With major advantages of high energy density, safer chemistries, low self-discharge, longer cycle life, broad temperature application, the li-ion batteries, availability in different form factors, are used in a range of applications like consumer electronics, automotive, space exploration, and medical implants [1,3], to name a few. With these growing applications in mind the health of the Li-ion battery becomes a critical factor in the combined system functionality of the device.

Faults occurring in the li-ion battery can be attributed to number of factors either individual, like structural failure, failure of thermal management, or more likely, a combination of factors involving manufacturing defects, over charge, over discharge, and short circuit. The currently available li-ion battery safety devices can be broadly divided into internal and external protection. The internal elements are implanted on the battery cell and provide protection against over current, high temperature, high pressure, over charge, and over discharge. The commonly used internal safety elements are the polymeric positive temperature coefficient (PPTC), charge interrupt devices (CID), and the printed circuit boards [4,5]. The external protection elements ensure the battery safety under over charge, overdischarge, and shorting through the use of devices like protection diodes, dedicated battery charging integrated circuit elements, temperature sensors, and more. Some of these devices are resettable while others are one time use, which later renders the battery useless. Furthermore, these protective devices fail to provide the user with any information regarding the condition of the battery, extent of the fault, fault identification, and battery

* Corresponding author.
E-mail addresses: soanwar@iupui.edu, anwar.sohel@gmail.com (S. Anwar).

http://dx.doi.org/10.1016/j.jpowsour.2014.06.052
0378-7753/

health prognosis. Critical insight into the battery health can be obtained by implementing analytical redundancy. It involves reconstructing the process behavior on-line by using models which mimic the actual process under study. The application of analytical redundancy for li-ion battery condition monitoring, fault detection and diagnosis results in better understanding of the battery dynamics, and hence contributes towards safer batteries, which leads to the overall system safety.

The application of fault detection and diagnosis on li-ion batteries is not new, extensive work in this area has been done by researchers with focus on different faults and related techniques. The work on li-ion battery fault detection is based primarily on the state estimation, empirical techniques, parameter identification, data driven methods and others.

Substantial work in the field of fault detection and diagnosis, and prognosis in li-ion battery using data driven methods has been carried out by Saha et al. [6–8]. Related research by using support vector machine algorithm for state of health (SOH) and remaining useful life (RUL) was recently carried out by Nuhic et al. [9] and Wang et al. [10]. These methods involve the application of classification and regression algorithms found under the paradigm of machine learning. In Ref. [11], the author uses AC impedance spectroscopy (IS) along with auto regressive moving average (ARMA), neural network, and fuzzy logic techniques for parameter identification, estimation and eventually battery prognosis. Data driven techniques do not require in depth knowledge of the battery and its underlying mechanisms, hence their implementation does not involve expert knowledge of the process under study. The biggest hurdle in using data driven methods can be attributed to the computational expensiveness and requirement of extensive data for training, and the time involved in learning.

A combination of rule based signal monitoring and probability based Li-ion battery fault detection and diagnosis was explored by Xiong et al. [12], these methods rely heavily on the thermal signatures of the battery which in turn depend on the rate of charge/discharge applied on the cell. Further, there is little information regarding the initial state of the cell under test; as it is difficult to achieve an over discharge cell failure in $LiFePO_4$ cell chemistries after two cycles. In Ref. [13], the open circuit voltage (OCV) is analyzed along with model based approach to detect the cell nominal capacity fade due to cycling. This technique gives good results for offline applications where the load can be disconnected and there is enough time to accurately access the OCV of a given cell.

Sate estimation involves the evaluation of the state of the battery, while the choice of technique can differ based on the requirements, the aim is to access the information related to the Li-ion battery that is not readily available through measurement [14]. The choice of state variable depends on the model of the system, but for Li-ion batteries, SOC among others is a natural candidate. Application of Luenberger observers (LO) for fault detection and diagnosis can be found in Ref. [15], here the authors implement fault diagnosis on a string of Li-ion batteries using a bank of reduced order observers. LO is a good candidate for fault detection and diagnosis in systems with little or no measurement noise, but with presence of noise, this setup will face inherent difficulties especially under subtle but important performance variation. The use of Kalman filters under the paradigm of observer based fault diagnosis for fault detection and diagnosis in Li-ion batteries is given in Ref. [16]. Where the optimal filter shows strong robustness to noise and the adaptive nature of the algorithm ensures accurate fault detection.

The use of observer based fault diagnosis under the paradigm of model based fault diagnosis offers inherent benefits like the decoupling of faults of interest from other faults, and minimizing the effects of unknown disturbances and model uncertainties [17]. These advantages are further utilized in the multiple model adaptive estimation (MMAE) technique; a special type of observer based fault diagnosis technique. MMAE employs a Kalman filter bank of n filters, where one observer represents the healthy condition of the process being monitored while the remaining $n-1$ observers represent the fault conditions of the process [16,18,19]. In addition to this apparent extension to the single observer case, MMAE also provides the added advantage of including a probabilistic approach to fault detection and diagnosis.

This paper is organized as follows: Section 2 describes the battery model, Section 3 describes the model-based fault diagnosis using nonlinear observers for residual generation and probability evaluation. Section 4 discusses the design of the experiment, and Section 5 provides the discussion of the results obtained. The conclusion of the work is captured in Section 6.

2. Battery modeling

Li-ion batteries can be modeled using different techniques namely electro chemical, neural networks, empirical, experimental and equivalent circuit [20,21]. The choice of modeling technique is a tradeoff between capturing cell dynamics and computational demand. For real time application the equivalent circuit model approach is adopted because it gives good representation of cell dynamics while maintaining low computational resource usage.

The Li-ion battery can be modeled as a third order system using lumped electrical elements like resistors and capacitors. The equivalent circuit model is shown in Fig. 1.where, R_b is the ohmic resistance, which accounts for the limited conductance of the metallic contacts, inter cell connections, electrode material and the bulk electrolytic resistance to electron and ion migration [1,22], constant phase element (CPE) C and resistance R are used to model the distribution of reactivity depicting the local property of the electrode., charge transfer resistance R_{ct} and double layer capacitance C_{dl} represent the interfacial impedance of the cell [23] and V_{OCV} represents the battery cell OCV. The CPE captures the distribution of reactivity at the electrodes which can be attributed to variation in surface properties. The impedance function of the combined RC pair is given by Refs. [23,24],

$$Z_{CPE}(\omega) = \frac{R}{1 + (j\omega)^{\alpha} QR} \tag{1}$$

where, α is the depression factor associated with the CPE and is assumed to be unity. As a result Q can be replaced by C and the CPE then behaves like a normal capacitor [22,23].

The circuit parameters depend on the SOC, temperature and capacity fade effects [25]. For this study, parameter dependency on these factors is assumed to be small. The effect of non-linear element in the equivalent circuit namely Warburg impedance representing the diffusion phenomenon is considered to be negligible [26].

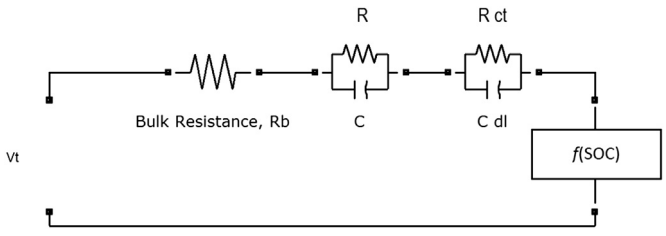

Fig. 1. Li-ion battery equivalent circuit model.

The function $f(\mathrm{SOC})$ represents the non-linear function that maps the relationship between the OCV and the SOC of the li-ion battery. This relationship is given by the classical OCV–SOC curve, as shown in Fig. 2.

The OCV–SOC data was recorded from a sample $LiFePO_4$ battery cell tested at room temperature at the Energy Systems and Power Electronics Laboratory (ESPEL) at IUPUI. Interested readers are directed to Ref. [27] for further reading on OCV–SOC relationship evaluation. Unlike the almost linear trend shown by lead acid batteries [1], the OCV–SOC profile for li-ion battery shows non-linear behavior with a relatively flat trend between 20 and 80% SOC. In cases where the OCV is used as an indicator of battery SOC, a small error in OCV evaluation can result in appreciable error in the resulting SOC. In addition, temperature along with age also has an effect on the OCV–SOC trend, and can cause it to shift.

The OCV–SOC relationship in Fig. 2 can be captured by a polynomial with varying degree and coefficients, resulting in different degrees of fit. A ninth degree polynomial is found to give the best fit and is selected. The non-linear function $f(\mathrm{SOC})$ is then given by,

$$f(\mathrm{SOC}) = a_9(\mathrm{SOC})^9 + a_8(\mathrm{SOC})^8 + a_7(\mathrm{SOC})^7 + a_6(\mathrm{SOC})^6 + a_5(\mathrm{SOC})^5 + a_4(\mathrm{SOC})^4 + a_3(\mathrm{SOC})^3 + a_2(\mathrm{SOC})^2 + a_1(\mathrm{SOC}) + a_0 \quad (2)$$

where $a_9 = 0.0385$, $a_8 = -0.01936$, $a_7 = -0.169$, $a_6 = 0.06142$, $a_5 = 0.2328$, $a_4 = -0.05715$, $a_3 = -0.08321$, $a_2 = 0.0005257$, $a_1 = 0.03205$, $a_0 = 3.297$.

From the equivalent circuit in Fig. 1, using Kirchhoff's voltage law, the rate of change in voltage across the capacitor C is given by,

$$\dot{V}_C = -\frac{V_C}{RC} + \frac{I_L}{C} \quad (3)$$

where V_C is the voltage across the capacitor C, and I_L is the battery load/charge current. The sign convention used in this study considers the negative sign of I_L as discharging while positive sign as charging. The rate of change in voltage across the double layer capacitor is given by,

$$\dot{V}_{C_{\mathrm{dl}}} = -\frac{V_{C_{\mathrm{dl}}}}{R_{\mathrm{ct}}C_{\mathrm{dl}}} + \frac{I_L}{C_{\mathrm{dl}}} \quad (4)$$

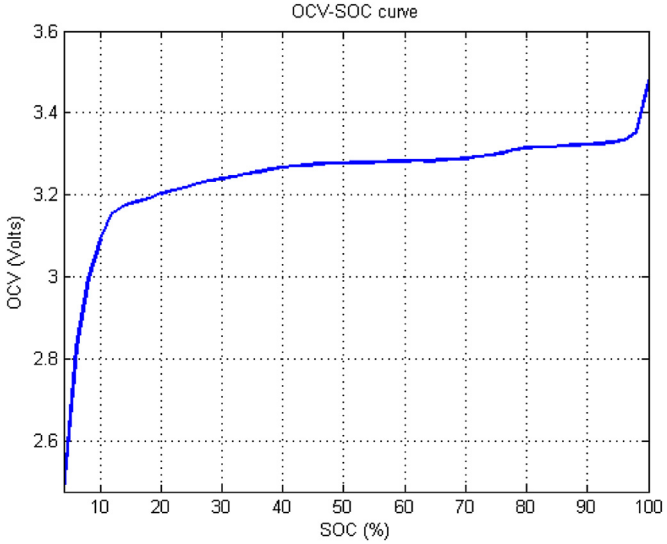

Fig. 2. Experimental OCV–SOC curve for $LiFePO_4$ battery cell.

where $V_{C_{\mathrm{dl}}}$ is the voltage across the double layer capacitor C_{dl}.

The SOC is defined as the ratio of the remaining capacity to the fully charged nominal capacity of the battery [28], and is given by,

$$\mathrm{SOC}(t) = \mathrm{SOC}(0) + \int_0^t \frac{\eta I_L(\tau)}{C_n} \mathrm{d}\tau \quad (5)$$

where $\mathrm{SOC}(0)$ represents the initial state of charge, C_n represents the battery cell nominal capacity in Ampere hour, η is the coulomb efficiency given by,

$$\eta = \begin{cases} 1, \text{charging} \\ 0.98, \text{discharging} \end{cases}$$

In discrete time, Eq. (5) can be given by,

$$\mathrm{SOC}(k) = \mathrm{SOC}(k-1) + \frac{\eta \Delta I_L(k)}{C_n} \quad (6)$$

where k is the time variable, and $\Delta I_L(k) = I_L(k) - I_L(k-1)$.

The discrete time versions of Eqs. (3) and (4) can be obtained by using zero-order hold (ZOH) process [29]. The transformed equations are given by,

$$V_C(k) = \left(e^{-\frac{\Delta t}{RC}}\right) V_C(k-1) + R\left[1 - \left(e^{-\frac{\Delta t}{RC}}\right)\right] I(k-1) \quad (7)$$

$$V_{C_{\mathrm{dl}}}(k) = \left(e^{-\frac{\Delta t}{R_{\mathrm{ct}}C_{\mathrm{dl}}}}\right) V_{C_{\mathrm{dl}}}(k-1) + R_{\mathrm{ct}}\left[1 - \left(e^{-\frac{\Delta t}{R_{\mathrm{ct}}C_{\mathrm{dl}}}}\right)\right] I(k-1) \quad (8)$$

The battery terminal voltage at any time sample k, is given by,

$$V_t(k) = f(\mathrm{SOC}) - I_L(k)R_b - V_C(k) - V_{C_{\mathrm{dl}}}(k) \quad (9)$$

where V_t is the battery terminal voltage, and $I_L R_b$ is the voltage drop across the bulk resistance R_b.

The state vector is given by $x_k = \begin{bmatrix} \mathrm{SOC}(k) & V_C(k) & V_{C_{\mathrm{dl}}}(k) \end{bmatrix}^T$ and the state equation for a non-linear time invariant system in discrete time is given by,

$$x(k) = g(x_{k-1},\ u_{k-1}) + w_{k-1} \quad (10)$$

and the output equation is given by,

$$z(k) = h(x_k, u_k) + v_k \quad (11)$$

where g and h are continuously differentiable non-linear functions, w is the process noise with zero mean and variance of,

$$E\left\{w_n[l]w_n^T[m]\right\} = \begin{cases} Q, & l = m \\ 0, & l \neq m \end{cases} \quad (12)$$

and v is the measurement noise, independent from w, with zero mean value as,

$$E\left\{v_n[l]v_n^T[m]\right\} = \begin{cases} R, & l = m \\ 0, & l \neq m \end{cases} \quad (13)$$

Q and R are the process and measurement noise variances respectively. The process and measurement white Gaussian noise is generated using the polar method [30].

From Eqs. (6)–(11), the functions g and h are given by,

$$g(k-1) = \begin{bmatrix} \mathrm{SOC}(k-1) + \dfrac{\eta \Delta t\ \mathrm{I}_L(\mathrm{k}-1)}{C_n} \\ \left(e^{-\frac{\Delta t}{RC}}\right) V_C(k-1) + R\left[1 - \left(e^{-\frac{\Delta t}{RC}}\right)\right] I(k-1) \\ \left(e^{-\frac{\Delta t}{R_{ct}C_{dl}}}\right) V_{C_{dl}}(k-1) + R_{ct}\left[1 - \left(e^{-\frac{\Delta t}{R_{ct}C_{dl}}}\right)\right] I(k-1) \end{bmatrix} \tag{14}$$

and

$$h(k) = f(\mathrm{SOC}) - I_L(k)R_b - V_C(k) - V_{C_{dl}}(k) \tag{15}$$

3. Model based fault diagnosis

The choice of diagnosis method is based on a combination of factors like cost, range of operation and complexity of process [17]. Software/analytical redundancy fault diagnosis is particularly important because it can be implemented at a low cost, incorporate process complexity and encompass range of system operation. Model based fault diagnosis is an integral part of software redundancy based fault diagnoses and is based on the process/physical model of the system. In the model based fault diagnosis scheme, the process model is the mathematical representation of the system. While this model should be able to show good agreement with the system dynamics of the process it should more importantly conform to the fault carrying dynamics of the process. Also for real time applications, a computationally inexpensive system representation will be advantageous as computational resources are limited; this consideration takes all the more precedence in mobile application. The measured output from the process is compared with the model response to generate the residuals. The performance of the model based fault diagnosis is further improved by replacing the process model and subsequent residual generation process with state observers [17,31,32], hence called the observer based fault diagnosis. This fundamental shift in residual generation process enables the removal of errors in the residual signal due to faulty initial condition, and unknown disturbances.

The general configuration of model based fault diagnosis with Kalman filter state observer is as shown in Fig. 3. The optimal filter works in parallel with the battery, and based on the measurements of load/charge current and the terminal voltage, it estimates the states of the battery model. The states are further utilized to generate the estimated terminal voltage $\hat{V}_t$. The fault/condition information carrying residuals are generated when the estimated terminal voltage is compared with the measured terminal voltage [16].

In the case of non-linear process models the Kalman filter in the observer based fault diagnosis is replaced by the extended Kalman filter.

3.1. Extended Kalman filter design

The Extended Kalman filters are used for state estimation of non-linear systems by linearizing around the current mean and covariance. When applied to the non-linear system of (10), (11), (14), and (15), the time update equations are given by Refs. [33,34],

$$\begin{aligned} \hat{x}_k^- &= g(\hat{x}_{k-1}, u_{k-1}) \\ P_k^- &= G_k P_{k-1} G_k^T + Q_{k-1} \end{aligned} \tag{16}$$

and the measurement update equations are given by,

$$\begin{aligned} K_k &= P_k^- H_k^T \left(H_k P_k^- H_k^T + R_k\right)^{-1} \\ \hat{x}_k &= \hat{x}_k^- + K_k\left(y_k - h\left(\hat{x}_k^-\right)\right) \\ P_k &= (I - K_k H_k) P_k^- \end{aligned} \tag{17}$$

where $\hat{x}_k^-$ represents predicted state based on the function g evaluated at the previously estimated state and available input, P_k^- is the *a priori* estimate error covariance, K_k is the Kalman gain, $\hat{x}_k$ is

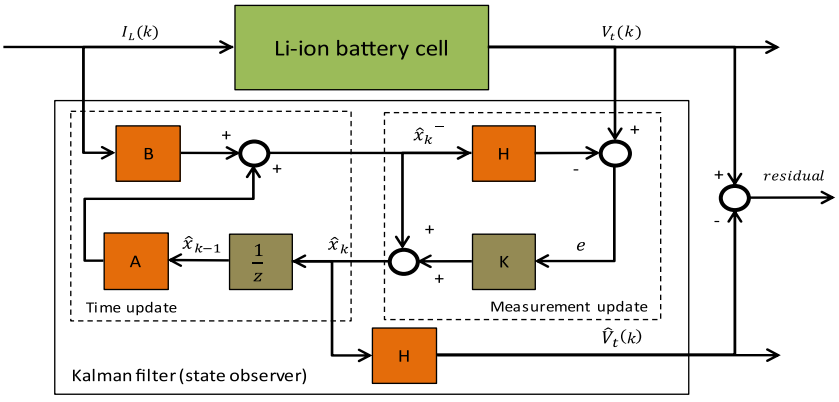

Fig. 3. Observer based fault diagnosis.

the updated state estimate and P_k is the updated covariance estimate. The state transition matrix G_k and observation matrix H_k are evaluated at each step and are given by,

$$G_k = \left.\frac{\partial g}{\partial x}\right|_{\hat{x}_{k-1}, u_{k-1}}$$
$$H_k = \left.\frac{\partial h}{\partial x}\right|_{\hat{x}_k^-, u_k} \quad (18)$$

The estimated terminal voltage is given by,

$$\hat{V}_t(k) = h(\hat{x}_k, u_k) \quad (19)$$

As mentioned earlier, the residual signal is obtained by subtracting the estimated terminal voltage signal from the measured terminal voltage of the battery and is given by,

$$r(k) = V_t(k) - \hat{V}_t(k) \quad (20)$$

where r is the fault/condition residual, V_t is the measured terminal voltage.

The single observer case, as shown in Fig. 3 can be extended to multiple observers with added advantages. Using a bank of extended Kalman filters, where each observer represents a particular fault/operational condition of the battery allows for robust li-ion battery monitoring covering a wide variety of operational conditions.

3.2. Multiple model adaptive estimation

MMAE is a special type of observer based fault diagnosis technique as it employs a Kalman filter bank (KFB) of n filters, where one observer represents the healthy condition of the process being monitored while the remaining $n-1$ observers represent the fault conditions of the process [16,19]. In addition to this apparent extension to the single observer case, MMAE also provides the added advantage of including a probabilistic approach to condition monitoring. The general layout of MMAE when applied to non-linear battery model with $n-1$ distinct operational conditions is as shown in Fig. 4.

The residual generation process involves non-linear observers which run parallel to the battery with all the n filters receiving the same input of load/charge current I_L and terminal voltage measurement V_t. The battery condition is continuously monitored and the n residuals are updated at each time instant. The post processing part involving the residual processing, decision logic and subsequent fault/condition declaration takes place at the conditional probability density evaluator block. At the conditional probability evaluator, each of the n fault/operational hypothesis is assigned a probability of being true. The probabilities range between 0 and 1 and the sum of all the n probabilities is equal to 1.

The earliest use of conditional probability density evaluation and weighting of coefficients can be found in Refs. [35–37], where the primary emphasis is the optimal state estimation and its applications. With respect to fault detection and diagnosis based implementation of Kalman filter and conditional probability density evaluation, extensive work has been done by Maybeck et al. [38–42] and Athans et al. [43] on the fault detection and diagnosis of aircraft systems.

The conditional probabilities require *a priori* samples to compute the current values and are normalized over a complete sum of conditional probabilities of all systems. The largest conditional probability among all can be used as an indicator of the fault/operational hypothesis being true. The probability for the n^{th} model at time sample k is given by,

$$P_{n,k} = \frac{f_{z(k)|a,Z(k-1)}(\boldsymbol{z}_k|\boldsymbol{a}_n, Z_{k-1}) p_n(k-1)}{\sum_{j=1}^{n} f_{z(k)|a,Z(k-1)}(\boldsymbol{z}_k|\boldsymbol{a}_j, Z_{k-1}) p_j(k-1)} \quad (21)$$

where $f_{z(k)|a,Z(k-1)}(\boldsymbol{z}_k|\boldsymbol{a}_n, Z_{k-1})$ is the conditional probability density function of the nth model considering the history of measurements $Z(t_{i-1}) = (z^T(t_1)\ldots z^T(t_{i-1}))$.

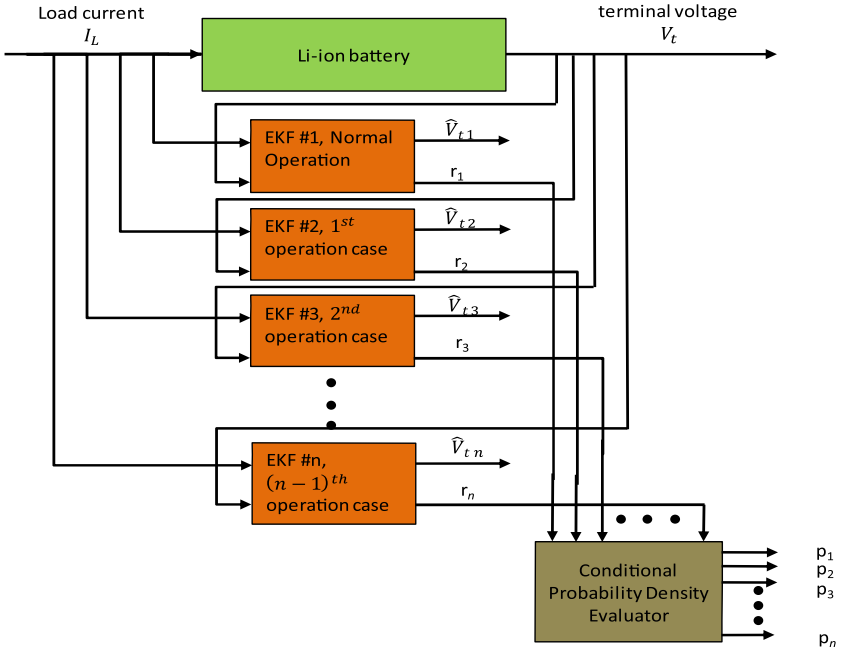

Fig. 4. MMAE residual generation and probability evaluation.

The conditional probability function is given by,

$$f_{z(k)|a,Z(k-1)}(\boldsymbol{z}_k|\boldsymbol{a}_n, Z_{k-1}) = \beta_n \exp(\circ) \tag{22}$$

$$V_t(k) = a_9(\mathrm{SOC})^9 + \ldots + a_0(\mathrm{SOC})^0 - I_L(k)R_b - V_C(k) - V_{C_{\mathrm{dl}}}(k) \tag{27}$$

separating the unknown parameters from the known signals, the parametric form for the battery model is given byt,

$$V_t(k) = \begin{bmatrix} a_9 & \ldots & a_0 & R_b & e^{-\frac{\Delta t}{RC}} & R\left(1-e^{-\frac{\Delta t}{RC}}\right) & e^{-\frac{\Delta t}{R_{\mathrm{ct}}C_{\mathrm{dl}}}} & R_{\mathrm{ct}}\left(1-e^{-\frac{\Delta t}{R_{\mathrm{ct}}C_{\mathrm{dl}}}}\right) \end{bmatrix}^T \times \begin{bmatrix} (\mathrm{SOC}(k))^9 & \ldots & (\mathrm{SOC}(k))^0 & -I_L(k) & -V_c(k-1) & -I_L(k-1) & -V_{C_{\mathrm{dl}}}(k-1) & -I_L(k-1) \end{bmatrix} \tag{28}$$

where

$$\beta_n = \frac{1}{(2\pi)^{l/2}\left|\psi_n(k)\right|^{1/2}} \tag{23}$$

l is the measurement dimension and equal to 1, since $V_t \in \mathbb{R}$.

$$(\circ) = -\frac{1}{2} r_{n,k}^T \psi_{n,k}^{-1} r_{n,k} \tag{24}$$

where $r_{n,k}$ is the residual signal for the nth model at time sample k. The covariance of the residual signal evaluated at each sample is given by,

$$\psi_{n,k} = C_{n,k} P_{n,k|k} C_{n,k}^T + R \tag{25}$$

where $C_{n,k}$ is the output vector for the nth system at any time sample k. For the non-linear battery model $C_{n,k} = \frac{\partial h}{\partial x}\Big|_{\widehat{x}_{k|k}}$, linearized output vector evaluated at the current estimated state. $P_{n,k|k}$ is the updated covariance update for nth model evaluated at kth sample, R is the measurement noise variance.

4. Design of experiments

In cases where the battery is subjected to cycles involving abusive charge or discharge, the battery undergoes a permanent change in its performance. The shift in battery performance induces a marked variation in model circuit parameters namely, the bulk resistance, constant phase elements, charge transfer resistance and the double layer capacitance, from their healthy battery counterparts. The parameter values of the battery under different condition is extracted using the recursive least squares technique [44].

4.1. Recursive least squares

The recursive least squares (RLS) system identification technique aims at fitting battery mathematical model to a sequence of observed battery current and voltage data by minimizing the sum of the squares of the difference between the observed and computed data recursively [44]. The system being identified is represented in the discrete time parameter form given by,

$$z(k) = \theta^{*T}\varphi \tag{26}$$

where z is the terminal voltage output, θ^* is the linear vector of unknown parameters that is being identified, ϕ is the vector of previous current and voltage measurements.

From Eqs. (9) and (2), the terminal voltage output is given by,

For further simplification, some of the parameters can be lumped together as shown below,

$$A_1 = e^{-\frac{\Delta t}{RC}}, B_1 = R\left(1-e^{-\frac{\Delta t}{RC}}\right), A_2 = e^{-\frac{\Delta t}{R_{\mathrm{ct}}C_{\mathrm{dl}}}}, B_2 = R_{\mathrm{ct}}\left(1-e^{-\frac{\Delta t}{R_{\mathrm{ct}}C_{\mathrm{dl}}}}\right) \tag{29}$$

The estimation equation is given by,

$$\theta(k) = \theta(k-1) + P(k)\varphi(k)\varepsilon(k) \tag{30}$$

where P is the covariance matrix, ε is the normalized estimation error, ϕ is the same as given in Eq. (26). At $k = 0$, $\theta(0)$ is the best initial guess on the parameters to be identified.

The normalized estimation error ε is given by,

$$\varepsilon(k) = \frac{V_t(k) - \theta(k)^T\varphi(k)}{m^2(k)} \tag{31}$$

where m^2 is the normalizing signal given by,

$$m^2(k) = cc + \varphi^T(k)\varphi(k) \tag{32}$$

with $cc > 0$, and $cc\varepsilon\mathbb{R}$

The covariance matrix P is updated recursively by using the following equation,

$$P(k) = P(k-1) - \frac{P(k-1)\varphi(k)\varphi(k)^T P(k-1)}{m^2(k) + \varphi(k)^T P(k-1)\varphi(k)} \tag{33}$$

with $P(0) = P_0 = P_0^T > 0$

4.2. Test setup

The li-ion battery selected for this study was A123 18650 $LiFePO_4$ (APR18650M 1A 3.3 V 1000 mAh) from A123 Systems (Cambridge, MA) [45]. The battery under test was subjected to nominal charge/overdischarge in a cyclic fashion. The overdischarge regime is based on Navy overdischarge cycle [46] and a 24 h overdischarge cycle. In the Navy over discharge cycle, the Li-ion battery is discharged at maximum suitable discharge rate for 25% over discharge. The charging of the battery is carried out using a standard non-abusive charge regime. The battery is cycled 25 times using this discharge-charge regime and the critical battery parameters are continuously monitored. In the 24 h over discharge test regime, the battery is discharged at a suitable discharge rate until the SOC reaches zero. To maintain near zero terminal voltage, a resistor is connected across the terminals for the duration of 24 h.

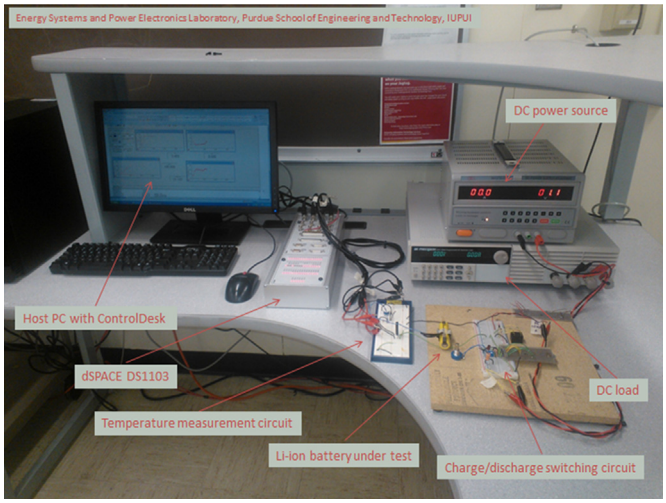

Fig. 5. Li-ion battery test setup.

The charging of the battery is then carried out using a standard non-abusive charging profile. The 24 h over discharge test cycle is repeated twice and the battery parameters are continuously monitored. The charging–discharging and data acquisition setup is as shown in Fig. 5.

In the test setup, a Mastech programmable DC power supply is used for charging of the battery, powering the charge–discharge switching circuit and the battery temperature measurement circuit. The BK Precision programmable DC electronic load is used to implement the dynamic discharge of the battery at the desired rates. The data acquisition is carried out using the dSPACE DS1103 board along with ControlDesk and the data post processing is implemented in MATLAB R2009 environment.

The recorded battery current and voltage data at the end of both test regimes is as shown in Fig. 6. The signals are filtered for noise using cascading low pass filters [47].

From the recorded current and voltage data of Fig. 6, the parameter values for the battery cell before and after the nominal charge/over discharge cycles are estimated. The identified system parameters are given in Table 1.

Table 1
Identified li-ion battery parameter values.

Parameter	New battery	Navy over discharge cycled battery	24 h Over discharge cycled battery
a^9	0.49161	0.748268	−0.02105
a^8	−0.08717	−0.07862	−0.04814
a^7	−0.32599	−0.42834	−0.00855
a^6	−0.27117	−0.37816	0.057027
a^5	−0.03456	−0.08725	0.092889
a^4	0.198062	0.201331	0.042196
a^3	0.206745	0.219284	−0.10774
a^2	−0.07741	−0.10596	−0.20669
a^1	−0.00024	−0.03705	0.341718
a^0	3.3558	3.490569	3.223314
R_b	−0.06492	−0.05705	−0.09248
A_1	0.241634	0.607614	0.216303
B_1	−0.06881	−0.06389	−0.09306
A_2	0.241634	0.034997	0.216303
B_2	−0.06881	−0.06389	−0.09306

Using the identified parameters, multiple battery condition representing models can be formulated. For the purpose of validation, the load current applied to condition monitoring setup is based on the urban dynamometer driving schedule (UDDS) drive cycle profile which has been appropriately scaled to match the nominal capacity of one cell. The UDDS drive cycle is accessed from Autonomie [48] and is represented in Fig. 7.

Three UDDS cycles are run back to back with the total testing duration of 213 s. While the load current profile simulates the actual working condition of the system, the resulting fault probabilities depend more on the zero average residual signal rather than the magnitude of the load current [16].

5. Diagnosis performance

To test the performance of the condition monitoring setup, a scenario is created with consecutive change in the battery condition. The total simulation time of 213 s is divided into four equal

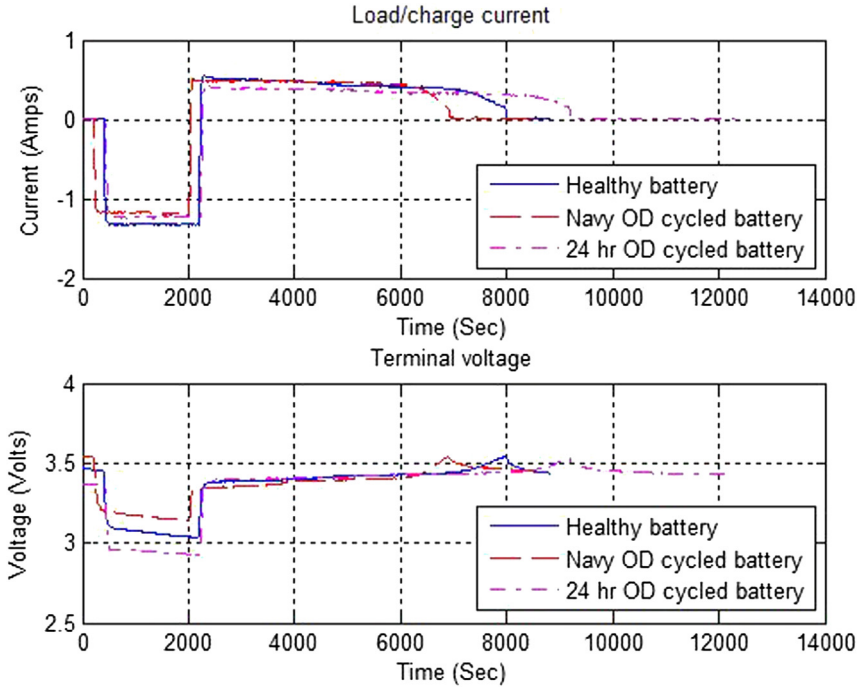

Fig. 6. Current and voltage profiles for healthy and nominal charge/overdischarge battery.

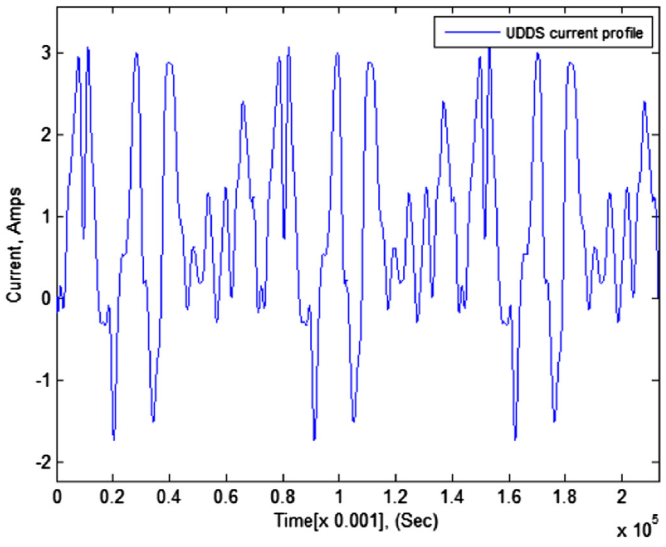

Fig. 7. Battery cell load current profile.

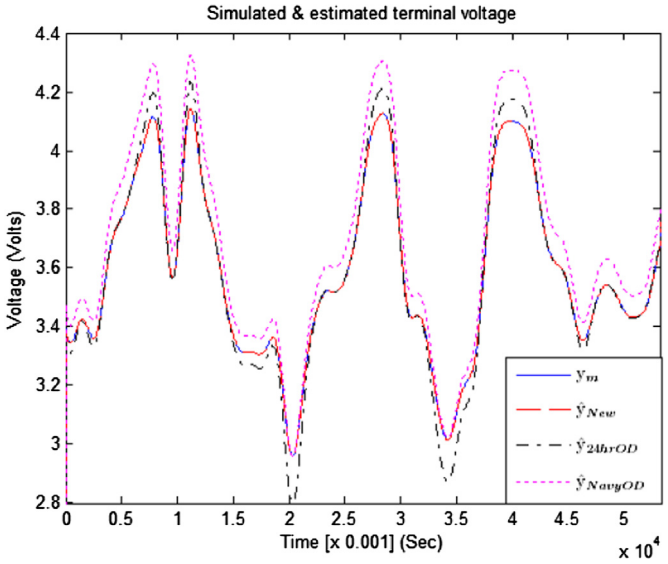

Fig. 9. Simulated and estimated terminal voltages: zero to 53.25 s.

parts, depicting the healthy and the deteriorated performance of the battery due to overdischarge. The condition change scenario is as given below,

- Zero to 53.25 s: healthy battery operation
- 53.26–106.5 s: battery operation after two 24 h overdischarge cycles
- 106.51–159.75 s: battery operation after twenty five Navy overdischarge cycles
- 159.76–213 s: healthy battery operation

Once the operational condition is diagnosed correctly, this setup helps to check the effectiveness of the condition monitoring algorithm to de-latch itself from its earlier diagnosis [49]. It is also assumed that only one type of fault can occur in the system at any given point in time. The starting SOC of the battery is considered to be at 70% and the polarization voltages are considered to be zero.

The UDDS load/charge current and the terminal voltage measurement embedded with the changing battery condition according to the scenario constructed above is made available to the three non-linear observers. The simulated terminal voltage measurement and observer outputs are as shown in Fig. 8.

Fig. 9 below shows the first section of the total simulated and estimated terminal voltages in Fig. 8.

The terminal voltage measurement y_m depicts the healthy battery operation and is shown by the continuous blue line in Fig. 9. For the duration of the first and last 53.25 s, the estimated terminal voltage for the healthy battery system, given by $\hat{y}_{\text{New}}$ shows good match with y_m while the estimated terminal voltages for the 24 h overdischarge $\hat{y}_{24\ \text{hr}OD}$, and Navy overdischarge $\hat{y}_{\text{Navy}OD}$ show marked deviation.

The second section capturing the terminal voltage signals from 53.26 to 106.5 s is as shown in Fig. 10.

In Fig. 10, $\hat{y}_{24\ \text{hr}OD}$ shows good match with y_m while $\hat{y}_{\text{Navy}OD}$ shows large deviation. $\hat{y}_{\text{New}}$ shows large deviation from y_m for

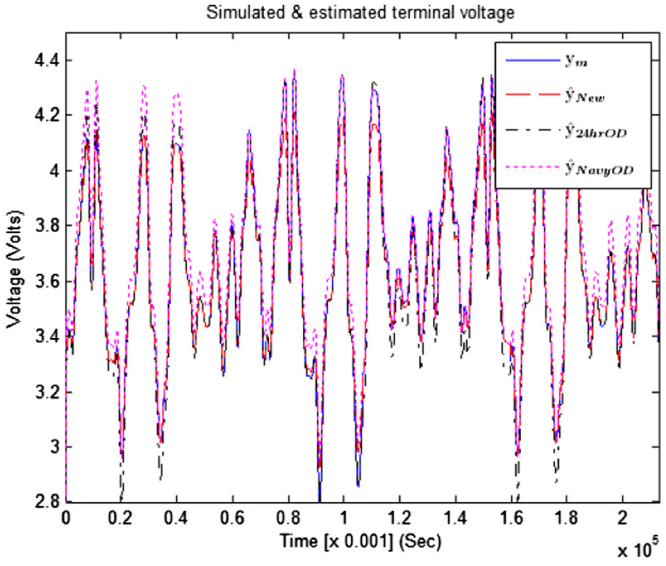

Fig. 8. Simulated and estimated terminal voltages.

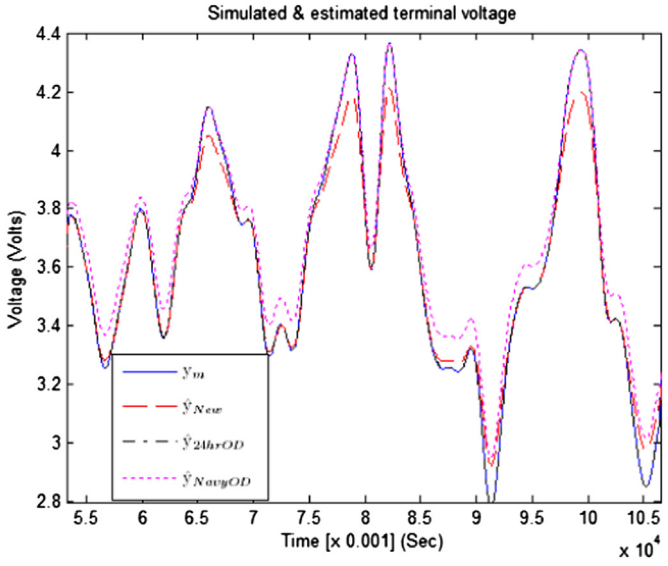

Fig. 10. Simulated and estimated terminal voltages: 53.26–106.5 s.

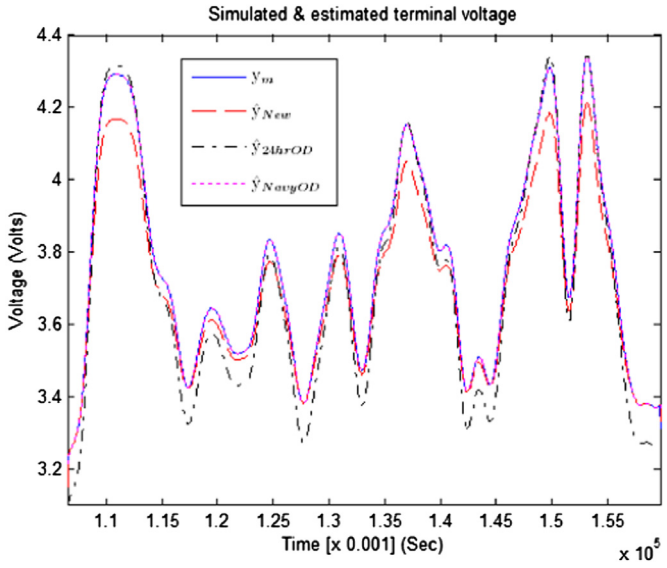

Fig. 11. Simulated and estimated terminal voltages: 106.51–159.75 s.

higher magnitudes of load/charge current. At smaller magnitudes of load/charge current, $\hat{y}_{New}$ is close to y_m but not as close as $\hat{y}_{24\ hrOD}$.

The third section of simulated and estimated terminal voltages is as shown in Fig. 11.

In Fig. 11, $\hat{y}_{NavyOD}$ shows good match with y_m while the other estimated terminal voltages $\hat{y}_{New}$ and $\hat{y}_{24\ hrOD}$ show large deviations from the simulated terminal voltage measurement.

The expected behavior shown by the estimated terminal voltage signals in Figs. 9–11 leads to system residuals as shown in Fig. 12. The residuals are evaluated using Eq. (20) and are updated at each time sample.

During the first and the last 53.25 s, the battery heath residual r_{new} shows a zero average behavior while 24 h overdischarge system residual $r_{24\ hr\ OD}$ and Navy overdischarge system residual $r_{Navy\ OD}$ show dynamic behavior within the same time durations. This response from the residuals shows that the healthy system operation is accurately captured. Similarly, from 53.26 to 106.5 s $r_{24\ hr\ OD}$ shows zero average behavior while other residuals show dynamic

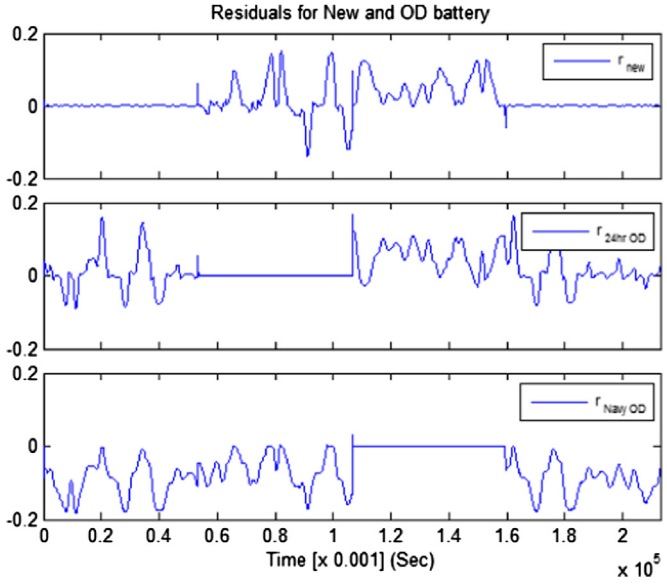

Fig. 12. System residuals for healthy and over discharged battery.

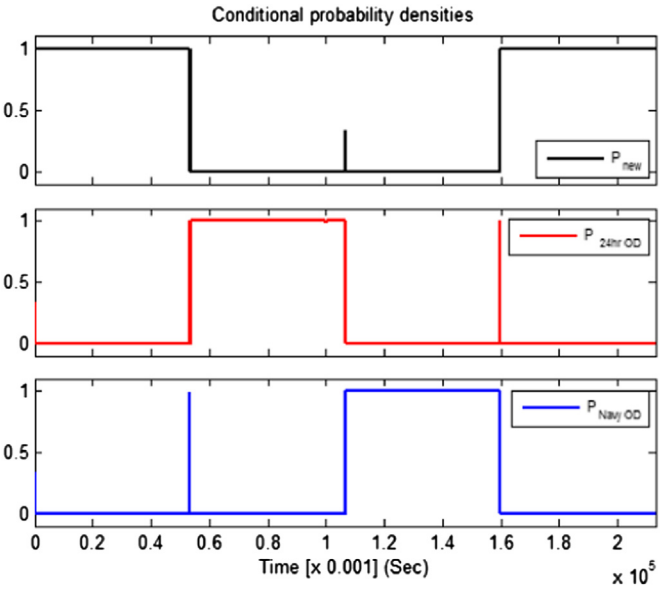

Fig. 13. Conditional probability densities for new and over discharged battery.

behavior, thus confirming the presence of 24 h overdischarge condition. With accurate state estimations, the same behavior can be seen for the residual $r_{Navy\ OD}$.

The residuals are evaluated using the probability density function and the normalized probabilities are updated at each time sample. The resulting battery condition probabilities are as shown in Fig. 13.

The 24 h overdischarge condition was injected at 53.25 s, which causes the battery health probability P_{new} to transition from 1 to 0, indicating the non-existence of healthy battery condition. The particular battery condition is further indicated by the probability $P_{24hr\ OD}$ increasing from 0 to 1. At the same time a spike in Navy overdischarge probability $P_{Navy\ OD}$ can be seen, this is because the probabilities can take some time to transition from one extreme state to another. The Navy overdischarge condition is correctly indicated at 106.51 s, where the condition probability $P_{Navy\ OD}$ transitions from 0 to 1 and $P_{24hr\ OD}$ drops from 1 to 0 while P_{new} remains at 0. Finally, at 159.76 s, the healthy battery condition is indicated by the probability P_{new} when it transitions from 0 to 1. At

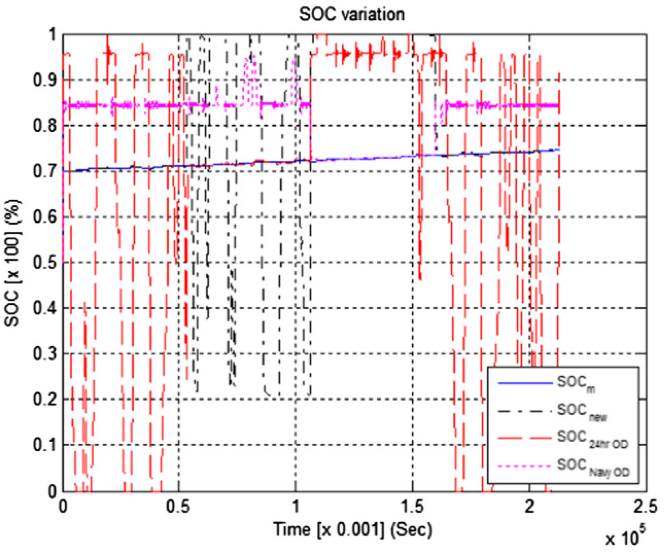

Fig. 14. SOC variation for healthy and over discharged battery conditions.

the same time $P_{\text{Navy } OD}$ drops from 1 to 0. The battery conditional probabilities show good and accurate behavior by detecting the correct battery condition at the correct time and also by avoiding intermediate loss in probability.

The SOC is one of the elements of the state of the non-linear battery model and contributes greatly towards accurate OCV estimation and thus the terminal voltage estimation. The variation of the simulated SOC measurement SOC_m using coulomb counting and the estimated SOC signals is as shown in Fig. 14.

For accurate condition monitoring of the li-ion battery it is imperative that the OCV is estimated accurately and is within reasonable limits. Inaccurate OCV estimation results in loss of critical battery condition information carried by the polarization voltages. To better approximate the actual operation, the SOC is bounded by 0% at bottom and 100% at the top.

In Fig. 14, during the first and the last 53.25 s, the estimated healthy battery SOC given by SOC_{new} matches with SOC_m while the estimated 24 h overdischarge SOC given by $SOC_{24hr\ OD}$ and the Navy overdischarge SOC given by $SOC_{Navy\ OD}$ show large deviation. From 53.26 to 106.5 s, $SOC_{24hr\ OD}$ shows good match with SOC_m while $SOC_{Navy\ OD}$ and SOC_{new} show large difference. Finally from 106.51 to 159.75 s $SOC_{Navy\ OD}$ closely follows SOC_m while SOC_{new} and $SOC_{24hr\ OD}$ show apparent deviation. Using the extended Kalman filters, the SOC is estimated with less than 1% accuracy within the appropriate region of battery condition.

6. Conclusion

In this paper an observer-based condition monitoring technique for a li-ion battery is developed and validated. Overdischarge in li-ion battery causes change in the operational characteristics of the battery which can be identified in real time using the proposed condition monitoring technique. The non-linear battery model parameters are extracted from the experimental voltage and current data pertaining to healthy and over discharged batteries. Bank of extended Kalman filters are used to access the internal dynamics of the battery cell and to estimate the internal condition of the electrochemical system. The effectiveness of the condition monitoring algorithm was tested by using two different overdischarge regimes on the li-ion battery, inducing different degree of battery condition deterioration. The developed condition monitoring technique showed robust performance by detecting the different degrees of overdischarge on the li-ion battery accurately.

References

[1] T.B. Reddy, Linden's Handbook of Batteries, vol. 4, McGraw-Hill, 2011.
[2] B. Scrosati, J. Garche, J. Power Sources 195 (2010) 2419–2430.
[3] M. Nagata, A. Saraswat, H. Nakahara, H. Yumoto, D.M. Skinlo, K. Takeya, et al., J. Power Sources 146 (8/26/2005) 762–765.
[4] I. Littelfuse, Use of Low Resistivity Surface Mount PPTC in Li-ion Polymer Battery Packs, 2012. Available: http://www.littelfuse.com/~/media/Electronics_Technical/Application_Notes/Resettable_PTCs/Littelfuse_Resettable_PTCs_LoRho_App_Note.pdf.
[5] M. Kahn, K. White, R.T. Long, Lithium-ion Batteries Hazard and Use Assessment, Springer, 2011.
[6] B. Saha, K. Goebel, S. Poll, J. Christophersen, An integrated approach to battery health monitoring using bayesian regression and state estimation, in: Autotestcon, 2007 IEEE, 2007, pp. 646–653.
[7] K. Goebel, B. Saha, A. Saxena, J. Celaya, J. Christophersen, Instrum. Meas. Mag. IEEE 11 (2008) 33–40.
[8] J. Liu, A. Saxena, K. Goebel, B. Saha, W. Wang, An Adaptive Recurrent Neural Network for Remaining Useful Life Prediction of Lithium-ion Batteries, DTIC Document, 2010.
[9] A. Nuhic, T. Terzimehic, T. Soczka-Guth, M. Buchholz, K. Dietmayer, J. Power Sources 239 (2013) 680–688.
[10] D. Wang, Q. Miao, M. Pecht, J. Power Sources 239 (2013) 253–264.
[11] J.D. Kozlowski, Electrochemical cell prognostics using online impedance measurements and model-based data fusion techniques, in: Aerospace Conference, 2003. Proceedings. 2003 IEEE, 2003, pp. 3257–3270.
[12] J. Xiong, H. Banvait, L. Li, Y. Chen, J. Xie, Y. Liu, et al., Failure detection for overdischarged Li-ion batteries, in: Electric Vehicle Conference (IEVC), 2012 IEEE International, 2012, pp. 1–5.
[13] M.A. Roscher, J. Assfalg, O.S. Bohlen, Veh. Technol. IEEE Trans. 60 (2011) 98–103.
[14] S.M. Alavi, M.F. Samadi, M. Saif, Diagnostics in Lithium-Ion batteries: challenging issues and recent achievements, in: Integration of Practice-oriented Knowledge Technology: Trends and Prospectives, Springer, 2013, pp. 277–291.
[15] W. Chen, W.T. Chen, M. Saif, M.F. Li, H. Wu, Control Syst. Technol. IEEE Trans. (2013), 1–1.
[16] A. Singh, A. Izadian, S. Anwar, Fault diagnosis of Li-Ion batteries using multiple-model adaptive estimation, in: Presented at the IEEE Industrial Electronics, IECON 2013–39th Annual Conference on, Vienna, Austria, 2013.
[17] S.X. Ding, Model-based Fault Diagnosis Techniques: Design Schemes, Algorithms, and Tools, Springer Publishing Company, Incorporated, 2008.
[18] A. Izadian, P. Khayyer, P. Famouri, Ind. Electron. IEEE Trans. 56 (2009) 973–978.
[19] A. Izadian, Mechatronics 23 (2013) 1094–1099.
[20] O. Tremblay, L.A. Dessaint, A.I. Dekkiche, A generic battery model for the dynamic simulation of hybrid electric vehicles, in: Vehicle Power and Propulsion Conference, 2007. VPPC 2007. IEEE, 2007, pp. 284–289.
[21] H. He, R. Xiong, J. Fan, Energies 4 (2011) 582–598.
[22] S. Buller, Impedance-based Simulation Models for Energy Storage Devices in Advanced Automotive Power Systems, Phd, Institute for Power Electronics and Electrical Drives, RWTH Aachen University, Germany, 2003.
[23] M.E. Orazem, B. Tribollet, Electrochemical Impedance Spectroscopy, John Wiley & Sons, Inc., 2008.
[24] E. Barsoukov, J.R. Macdonald, Impedance Spectroscopy: Theory, Experiment, and Applications, Wiley, 2005.
[25] S. Buller, M. Thele, R.W.A.A. De Doncker, E. Karden, Ind. Appl. IEEE Trans. 41 (2005) 742–747.
[26] T.C. Kaypmaz, R.N. Tuncay, An advanced cell model for diagnosing faults in operation of Li-ion polymer batteries, in: Vehicle Power and Propulsion Conference (VPPC), 2011 IEEE, 2011, pp. 1–5.
[27] S. Abu-Sharkh, D. Doerffel, J. Power Sources 130 (5/3/2004) 266–274.
[28] M. Ehsani, Y. Gao, A. Emadi, Modern Electric, Hybrid Electric, and Fuel Cell Vehicles: Fundamentals, Theory, and Design, second ed., Taylor & Francis, 2009.
[29] K. Ogata, Discrete-time Control Systems, Prentice Hall, Englewood Cliffs, N.J, 1995.
[30] S.M. Ross, A First Course in Probability, Pearson Prentice Hall, 2010.
[31] R. Isermann, Fault-diagnosis Applications: Model-based Condition Monitoring: Actuators, Drives, Machinery, Plants, Sensors, and Fault-tolerant Systems, Springer, 2011.
[32] R. Isermann, Fault-diagnosis Systems: an Introduction from Fault Detection to Fault Tolerance, Springer, 2006.
[33] W. Greg, B. Gary, An Introduction to the Kalman Filter, Department of Computer Science, University of North Carolina, Chapel Hill, NC, 2006.
[34] B.D.O. Anderson, in: J.B. Moore (Ed.), Optimal Filtering, Prentice-Hall, Englewood Cliffs, N.J, 1979.
[35] D. Magill, Optimal adaptive estimation of sampled stochastic processes, in: Automatic Control, IEEE Transactions, vol. 10, 1965, pp. 434–439.
[36] J. Moore, R. Hawkes, Decision methods in dynamic system identification, in: Decision and Control Including the 14th Symposium on Adaptive Processes, 1975 IEEE Conference on, 1975, pp. 645–650.
[37] D. Lainiotis, Optimal adaptive estimation: structure and parameter adaption, in: Automatic Control, IEEE Transactions, vol. 16, 1971, pp. 160–170.
[38] P.S. Maybeck, D.L. Pogoda, Multiple model adaptive controller for the stol f-15 with sensor/actuator failures, in: Decision and Control, 1989., Proceedings of the 28th IEEE Conference on, 1989, pp. 1566–1572.
[39] D.W. Lane, P.S. Maybeck, Multiple model adaptive estimation applied to the LAMBDA URV for failure detection and identification, in: Decision and Control, 1994., Proceedings of the 33rd IEEE Conference on, vol. 1, 1994, pp. 678–683.
[40] P. Eide, P. Maybeck, Implementation and demonstration of a multiple model adaptive estimation failure detection system for the F-16, in: Decision and Control, 1995., Proceedings of the 34th IEEE Conference on, vol. 2, 1995, pp. 1873–1878.
[41] T.E. Menke, P.S. Maybeck, Multiple model adaptive estimation applied to the VISTA F-16 flight control system with actuator and sensor failures, in: Aerospace and Electronics Conference, 1992. NAECON 1992., Proceedings of the IEEE 1992 National, 1992, pp. 441–448.
[42] P.D. Hanlon, P.S. Maybeck, Aerosp. Electron. Syst. IEEE Trans. 36 (2000) 393–406.
[43] M. Athans, D. Castanon, K.-P. Dunn, C. Greene, W. Lee, N. Sandell Jr., et al., Autom. Control IEEE Trans. 22 (1977) 768–780.
[44] P. Ioannou, B. Fidan, Adaptive Control Tutorial, Society for Industrial and Applied Mathematics, 2006.
[45] A. Systems, High Power Li-Ion APR18650 [Data Sheet], 2009. Available: www.cosmoenergy.com/APR18650M1A_Datasheet_2009.pdf.
[46] D. o. t. Navy, Technical Manual for Batteries, Navy Lithium Safety Program Responsibilities and Procedures, 2004.
[47] F. Richard, D. Beasley, Theory and Design for Mechanical Measurements, 2011.
[48] ANL, Autonomie, Argonne National Laboratory, 2010.
[49] A. Izadian, P. Famouri, Control Syst. Technol. IEEE Trans. 18 (2010) 1233–1240.